

QCD-Like Theories with Different Color Numbers

Toru Kojo^a

^aTheory Center, IPNS, High Energy Accelerator Research Organization (KEK), 1-1 Oho, Tsukuba, Ibaraki, 305-0801, Japan

© 20xx Elsevier Ltd. All rights reserved.

Chapter Article tagline: update of previous edition., reprint..

Glossary

Hadrons composite color-singlet states of quarks and gluons bound by the strong interaction.

Nuclear forces effective interactions between baryons arising from underlying quark and gluon dynamics.

Sign problem the difficulty in Monte Carlo simulations of QCD at finite baryon density, caused by the complex fermion determinant.

Quark-hadron crossover a smooth transition between hadronic and quark matter without a genuine thermodynamic phase transition.

Quarkyonic matter a hypothetical phase of QCD characterized by a quark Fermi sea coexisting with confining gluodynamics.

Chiral Perturbation Theory (ChPT) a low-energy effective field theory of QCD based on the spontaneous breaking of chiral symmetry.

Nomenclature

N_c	Number of colors
N_f	Number of flavors
μ_q	Quark chemical potential
μ_B	Baryon chemical potential ($= N_c \mu_q$)
n_0	nuclear saturation density $\simeq 0.16 \text{ fm}^{-3}$ ~ nucleon density in typical nuclei
EOS	Equations of state
NG bosons	Nambu-Goldstone bosons
QC ₂ D	Two-color QCD
QCD ₁	QCD at finite isospin but zero baryon density
BEC	Bose-Einstein condensation
BCS	Bardeen-Cooper-Schrieffer
pQCD	Perturbative QCD

Abstract

Quantum chromodynamics (QCD) with a general number of colors, N_c , provides a powerful theoretical laboratory to explore the dynamics of non-Abelian gauge theories. Although $N_c = 3$ does not look a large number, the $1/N_c$ expansion provides us with a very useful classification and book-keeping scheme for hadronic processes and sharpens conceptions otherwise obscured in real-world QCD with $N_c = 3$. Important applications are dense QCD matter where the first principle methods for QCD are not available and many conceptual issues remain to be clarified. In this chapter we first review hadrons at large N_c from the viewpoint of quark-gluon dynamics, and then extend the discussions to hot/dense matter, focusing on confinement-deconfinement aspects. We emphasize how the large- N_c limit provides a unified organizing principle for hadronic and quark degrees of freedom in regimes where first-principle methods are limited. Two-color and isospin QCD, for which lattice simulations at finite density can be performed for a special reason, is reviewed.

1 Introduction

Quantum chromodynamics (QCD) with a general number of colors, N_c , provides a powerful theoretical laboratory to explore the dynamics of non-Abelian gauge theories, including confinement, chiral symmetry breaking, and the structure of hadrons. By varying the number of colors N_c , one can uncover systematic patterns and scaling laws that are otherwise obscured in real-world QCD with $N_c = 3$. This strategy was originally introduced by 't Hooft (['t Hooft, 1974](#)).

Although $N_c = 3$ does not look a large number, the $1/N_c$ expansion provides us with a very useful classification scheme for hadronic processes and in practice it often works remarkably well. This seemingly unreasonable success suggests that the coefficients of the $1/N_c$ expansion are numerically small in many physically relevant situations. A similar situation occurs in quantum electrodynamics; although the elementary charge $e \simeq 0.27$ is not very small, in loop computations the coupling e appears in powers of $\alpha_e = e^2/4\pi \simeq 1/137$, a very small number ([Witten, 1980](#); [Coleman, 1985](#)). Another example is the critical exponent ν in the 3D Ising model; in the expansion $\epsilon = 4 - d$ ($d = 3$: spatial dimension), one gets $\nu = 1/2 + \epsilon/12 + O(\epsilon^2)$ with which $\nu(\epsilon = 1) \simeq 0.583$, reasonably close to the experimental value $\nu_{\text{exp}} \simeq 0.630$ ([Wilson and Fisher, 1972](#)). In this spirit, it would even make sense to study $N_c = 2$ theories as approximate laboratories for the real-world

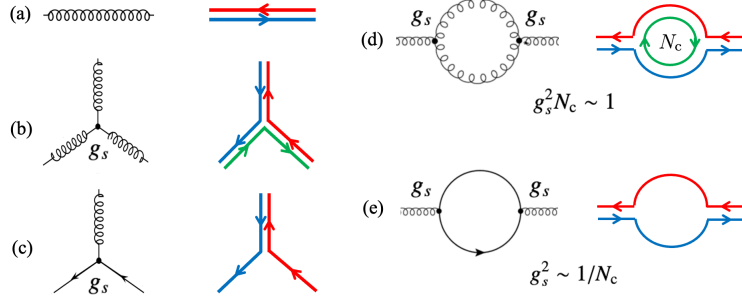


Fig. 1 Double-line representation and large- N_c counting rules. (a)–(c) Fundamental interaction vertices. (d) Planar gluon loop giving a factor N_c with $g_s^2 N_c \sim 1$ fixed. (e) Non-planar contraction suppressed as $g_s^2 \sim 1/N_c$.

QCD.

An expansion in powers of $1/N_c$ is a method of utility to classify various processes in hadron physics (Callan et al., 1976; Witten, 1980). This can be done by matching the quark-gluon graphs with hadronic graphs. The matching explicitly takes into account the fact that quarks are constituents of hadrons and also mediators of hadron-hadron interactions. From this viewpoint, there should be a unified framework for the hadronic structure and hadron-hadron interactions.

In terms of $1/N_c$ expansion, the decay width of a meson, Γ , divided by its mass m so as to cancel the phase space factor, is estimated to be $\Gamma/m \sim 1/N_c$. Thanks to this small width compared to its mass, one can treat mesons as if quasi-particles; if the width were as large as the mass, there would be no point to construct effective models of those very unstable mesons. This sort of counting may be extended to the estimate for meson-meson interactions, which are $\sim N_c^{-1/2}$ for three-meson vertices, $\sim N_c^{-1}$ for four-meson vertices, and so on. This leads to a picture that mesons are weakly interacting hadrons.

The application to the baryon sector is less straightforward than the mesonic sector, but it still provides us with a useful guide (Witten, 1980). In particular, the strong channel dependence of baryon-baryon interactions can be vividly characterized in powers of N_c (Kaplan and Savage, 1996). Provided that the quark-meson coupling is $\sim N_c^{-1/2}$, the baryon-meson coupling depends on how the quark-meson couplings are assembled. When N_c -quarks contribute constructively, the baryon-meson coupling is $\sim N_c^{-1/2} \times N_c \sim N_c^{1/2}$ which is strong. Meanwhile when N_c -quarks contribute destructively, the baryon-meson coupling is $\sim N_c^{-1/2} \times 1 \sim N_c^{-1/2}$. In terms of baryon-baryon forces, the overall strength is proportional to the square of the vertices, so the former is $\sim N_c$ and the latter is $\sim 1/N_c$; there is a factor $N_c^2 \sim 10$ difference. This large hierarchy is indeed seen in the meson exchange potentials (e.g., Stoks et al. (1994)).

The $1/N_c$ expansion provides particularly valuable guidance in discussing QCD matter at finite temperature and density. One of contemporary problems in quantum chromodynamics (QCD) is to understand transitions from a matter of hadrons to those of quarks and gluons (for a review, e.g., Fukushima and Hatsuda (2011)). These hadronic estimates are building blocks to consider such transitions. In the dilute regime, quarks and gluons are confined into hadrons so that the properties of a matter may be understood in terms of the hadronic language. This situation changes in the hot/dense regime where hadrons strongly interact and/or spatially overlap so that quarks and gluons become natural effective degrees of freedom to characterize the medium. Many key questions in hot and dense QCD are associated with this intermediate regime, where neither purely hadronic nor weakly coupled quark-gluon descriptions are sufficient.

Expanding our scope to QCD with a general number of colors, two-color QCD (QC₂D) provides a theoretical laboratory for studying nonperturbative aspects of QCD. One of the distinct properties of this system is that, unlike real-world QCD, lattice Monte Carlo simulations can be performed at finite baryon density (Hands et al., 1999). In fact, over the last decade, lattice simulations of dense QC₂D have confirmed several concepts of dense matter that were originally inferred from neutron star observations (Iida and Itou, 2022). Although there is an important difference between QC₂D and QCD in that a baryon is a boson in the former and a fermion in the latter, in sufficiently dense regimes where baryons overlap and quark degrees of freedom become manifest, it is reasonable to expect that the resulting matter shares qualitative similarities in these two theories. A similar strategy can also be applied to QCD with a finite isospin chemical potential (QCD_I), for which lattice simulations are likewise applicable (Brandt et al., 2023; Abbott et al., 2023).

In this chapter, we will review the basics and applications of QCD with a general N_c . After briefly summarizing the basics of $1/N_c$ expansion, we apply the framework to classifications of hadronic processes. The hadronic estimates are subsequently used to study many-hadron systems, and then extended to the studies of hot/dense matter. We also discuss QC₂D and QCD_I by referring to recent lattice results and model studies. Throughout this chapter, we emphasize qualitative patterns and physical intuition, and refer the reader to the original literature for technical details.

2 The $1/N_c$ expansion: definition

In 't Hooft large N_c limit, we take N_c large while holding $\lambda = N_c g_s^2$ fixed ('t Hooft, 1974). Here g_s is the gauge coupling constant. This condition on g_s^2 comes from the requirement that the running $\alpha_s = g_s^2/4\pi$ in large N_c QCD behaves in the similar way as QCD. Explicitly,

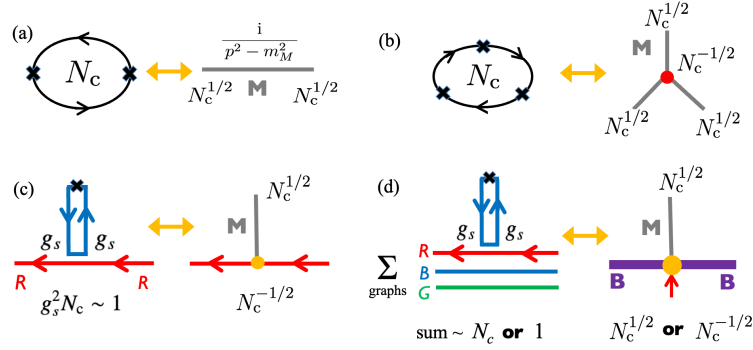


Fig. 2 Large N_c matching between quark-gluon and hadronic graphs. (a) Matching of the meson two-point function, which fixes the state-operator coupling $\langle M|\bar{q}\Gamma q|0\rangle \sim N_c^{1/2}$. (b) Meson three-point interaction whose vertex scales as $N_c^{-1/2}$. (c) Quark-meson coupling determined to be $N_c^{-1/2}$. (d) Baryon-meson coupling scaling as $N_c^{1/2}$ or $N_c^{-1/2}$, depending on whether quark-meson graphs add constructively or destructively.

the running α_s at one-loop level scales as

$$\alpha_s(Q^2) = \frac{4\pi}{\beta_0 \ln(Q^2/\Lambda_{\text{QCD}}^2)}, \quad \beta_0 = \frac{11N_c - 2N_f}{3}, \quad (1)$$

where N_f is the number of flavors and $\Lambda_{\text{QCD}} \simeq 200\text{-}300$ MeV is the typical nonperturbative scale in QCD. In QCD, there are $\sim N_c^2$ gluons and $\sim N_c N_f$ quarks. In the large N_c limit ($N_c \gg N_f$), the dynamics is dominated by gluons and the impact of quarks are treated as corrections.

It is convenient to use color line representation for the Feynman diagrams. The gluon fields A_a ($a = 1, \dots, N_c^2 - 1$) as the adjoint representations of $SU(N_c)$ may be rewritten as $A_j^i \equiv A_a(T_a)_j^i$ where matrices T_a form $SU(N_c)$ algebra and one may use the combinations of $i, j = 1, \dots, N_c$ to specify the gluon species. Using the indices i, j , one can keep track of the color charges which are conserved. For instance, a gluon propagator can be written as (Fig. 1(a)).

$$\langle (A_\mu)_j^i(x) (A_\nu)_l^k(0) \rangle = \langle A_\mu^a(x) A_\nu^b(0) \rangle \times (T_a)_j^i (T_b)_l^k = D_{\mu\nu}(x) \times (T_a)_j^i (T_a)_l^k = D_{\mu\nu}(x) \times \frac{1}{2} \left(\delta_j^i \delta_l^k - \frac{1}{N_c} \delta_j^i \delta_l^k \right), \quad (2)$$

where we used $\langle A_a(x) A_b(0) \rangle = D(x) \delta_{ab}$. The Kronecker δ in the last expression reflects how colors are transferred. The last $1/N_c$ term comes from the difference between $SU(N_c)$ and $U(N_c)$. This difference is usually negligible.

Likewise, the color conservation at three-gluon vertices can be represented as (Fig. 1(b))

$$f_{abc} (\partial_\mu A_\nu^a) A_\alpha^b A_\beta^c = 2i (T_b)_j^i (T_c)_i^k - (T_c)_k^j (T_b)_i^k \times (\partial_\mu A_\nu^a) A_\alpha^b A_\beta^c = 2i (\partial_\mu A_\nu^a)_j^i [(A_\alpha)_k^j (A_\beta)_i^k - (A_\beta)_k^j (A_\alpha)_i^k]. \quad (3)$$

The four-gluon vertex can be discussed in the similar way. As for the color transfer between gluons and quarks, the usual quark-gluon coupling may be rewritten as (suppressing the γ -matrices, Fig. 1(c))

$$\bar{q}_a T_a q = \bar{q}_i \partial A_a (T_a)_i^j q^j = \bar{q}_i A_i^j q^j. \quad (4)$$

From the contraction of the indices, one can see how the colors carried by quarks and antiquarks are transferred to gluons. After establishing the color conservation, one can assign N_c counting for various graphs for interaction processes.

To discuss loop corrections, we first consider graphs including only gluon lines (e.g., Fig. 1(d) for one-gluon loop). Since $g_s \sim N_c^{-1/2}$, increasing the order of g_s introduces more suppression factors. Meanwhile, in loop computations there appear graphs in which color lines are contracted by themselves, forming loops. Since loops may be formed for any colors, the color loops introduce an enhancement factor N_c . When we consider the so-called planar graphs in which all color lines may be drawn on a plane, at any order of loops g_s^2 appears together with the enhancement factor N_c , so that $g_s^2 N_c \sim 1$ contribute at the same order of N_c as graphs with less number of loops. That is, all planar graphs contribute equally in terms of the $1/N_c$ expansion. Meanwhile, if the graphs contain non-planar lines, we have less color line contraction and hence lose the enhancement factor N_c , see 't Hooft (1974) for those examples. Those graphs are regarded as sub-leading.

Next we include quarks (Fig. 1(e)). It is instructive to consider one loop correction from gluons and quarks to a gluon propagator. As we have just discussed above, gluon loops connect one index with the external line and contract the other index to generate a color loop with the N_c enhancement. A quark loop does not have such N_c enhancement, and hence is smaller than the gluon loop by a factor $\sim 1/N_c$. Every time we replace a gluon loop with a quark one, the graph acquires the suppression factor $\sim 1/N_c$.

3 Mesons at large N_c

Based on the N_c counting in the previous section, we now consider matching between quark-gluon graphs and hadronic graphs. Our first step is to consider a correlation function $\langle 0|J_M(x)J_M^\dagger(0)|0\rangle$ with J_M being a color singlet quark bilinear operator $\bar{q}\Gamma q$ (Fig. 2(a)). In the color

4 QCD-Like Theories with Different Color Numbers

line representation, the correlation function includes a color loop and is estimated to be $\sim N_c$. On the other hand, in the hadronic language J_M^\dagger creates a hadronic state $|n\rangle$, and this state evolves in time, and then get annihilated by the operator J_M . Taking the Fourier transform, our matching can be expressed as

$$\int_x e^{ipx} \langle 0 | J_M(x) J_M^\dagger(0) | 0 \rangle \sim N_c \sim \sum_n \langle 0 | J_M(0) | n(\vec{p}) \rangle \frac{i}{p^2 - m_n^2} \langle n(\vec{p}) | J_M^\dagger(0) | 0 \rangle. \quad (5)$$

From this matching, one can estimate the state-operator coupling $\langle n(\vec{p}) | J_M^\dagger(0) | 0 \rangle$ to be $\sim N_c^{1/2}$.

Our next step is to examine the N_c counting for meson vertices. We begin with three meson vertices (Fig. 2(b)). We consider a three point function among three interpolating fields J_{M_i} with $i = 1, 2, 3$. In quark-gluon graphs, this simply forms a single color loop and hence is estimated to be $\sim N_c$. To match this counting in terms of hadronic graphs, each state-operator coupling is $\sim N_c^{1/2}$ so that the three meson vertex must scale as $N_c^{-1/2}$. With this weak coupling, processes such as a decay process $M_1 \rightarrow M_2 M_3$ or a fusion process $M_1 M_2 \rightarrow M_3$ are suppressed at large N_c .

More quantitatively, squaring the former amplitude for a meson n , we estimate the width Γ_n to be $\sim 1/N_c$ times a factor depending on the phase space available for decays. Since the phase space factor depends on the overall mass scale, it is appropriate to look at the ratio Γ_n/m_n where the phase space factor is largely cancelled. For instance, the ratio for $\rho(770)$ with $m_\rho \simeq 775$ MeV and $\Gamma_\rho \simeq 150$ MeV is $\Gamma_\rho/m_\rho \sim 0.2$; for $\omega(782)$, $\Gamma_\omega/m_\omega \sim 0.011$; for $K^*(892)$, $\Gamma_{K^*}/m_{K^*} \sim 0.06$. Even $a_1(1260)$ with the apparently large decay width $\Gamma_{a_1} \sim 250\text{-}600$ MeV, the ratio $\Gamma_{a_1}/m_{a_1} \sim 0.2\text{-}0.5$ is not so bad. These small ratios $\Gamma_n/m_n \sim 1/N_c \ll 1$ allow us to regard mesons as quasi-particles and to employ an effective mesonic Lagrangian as an approximate framework. (Actually there are also exceptional mesons which significantly violate these estimates — they are often called exotics, see, e.g., [Pelaez \(2004\)](#); [Weinberg \(2013\)](#)).

Next we consider four meson vertices. The straightforward extension of the three vertex case allows us to estimate the four-meson vertex to be N_c^{-1} . Every time we attach an additional meson line, the strength of the vertex is suppressed by an extra factor $N_c^{-1/2}$. As a result, meson theories in the large N_c limit become weakly interacting theories.

4 Baryons at large N_c

The utility of the $1/N_c$ expansion in the baryon sector is less firmly established than in the meson sector. In particular, baryons have the masses of $\sim N_c$, and their internal structure and interactions are more sensitive to dynamical details.

4.1 Baryon-meson coupling

In this section, we begin with baryon–baryon interactions. The classification of baryonic interactions in powers of $1/N_c$ provides a useful organizing principle ([Witten, 1980](#)) and captures several qualitative aspects of nuclear forces ([Kaplan and Savage, 1996](#)).

First we note that the quark-meson coupling is $N_c^{-1/2}$ (Fig. 2(c)). To see this, we consider a diagram in which an interpolating field J_M couples to two external quark lines. For simplicity we consider a graph with one gluon exchange. There is a color loop yielding a factor N_c , and two quark-gluon vertices introduce $g_s^2 \sim N_c^{-1}$ so that this graph is ~ 1 as a total. As a hadronic graph, the state-operator coupling is $\sim N_c^{1/2}$ so that the quark meson coupling must be $\sim N_c^{-1/2}$.

To estimate baryon-meson couplings, we sum up graphs in which a meson line is attached to one of N_c quarks in a baryon (Fig. 2(d)). The consequence of the summation strongly depends on the channel we consider. The baryon-meson coupling is strong when each quark contribution is added constructively; in this case there is a factor N_c enhancement so that the baryon-meson coupling constant is large, $g_{BBM}^{\text{constructive}} \sim N_c^{-1/2} \times N_c \sim N_c^{1/2}$. Meanwhile, there are also channels in which quark contributions are added destructively; in this case there is no N_c enhancement and the baryon-meson coupling constant remains small, $g_{BBM}^{\text{destructive}} \sim N_c^{-1/2} \times 1 \sim N_c^{-1/2}$. In meson exchange potentials, its strength is $\sim g_{BMM}^2$, so that the ratio $1/N_c$ in couplings is enlarged to the $1/N_c^2$ difference in the corresponding potentials.

A useful example is the difference between ω and ρ exchange potential between two nucleons. They appear in the form $\sim g_{\omega NN} \omega_0 \bar{N} \gamma_0 N$ and $\sim g_{\rho NN} \rho_0^a \bar{N} \gamma_0 \tau_a N$. Here we consider the temporal or electric components of these mesons for which we use ω_0 and ρ_0 in our notation. The ω_0 couples to the quark numbers carried by the baryon and there is N_c enhancement since all quarks have positive quark/baryon number. The situation differs for the ρ_0 meson, as it couples to the isospin charge of a nucleon which is ~ 1 in the N_c counting. Nucleons have both u - and d -quarks and they have opposite isospins, so that contributions with the opposite signs cancel. More quantitatively, in a representative meson exchange potential (e.g., [Stoks et al. \(1994\)](#)), the ratio $g_{\omega NN}/g_{\rho NN}$, evaluated so as to cancel the form-factor dependence, is found to be $g_{\omega NN}/g_{\rho NN} \sim 3.3$. This value is consistent with the expectation from the large N_c counting.

Another illustrative example is given by the σ and $a_0(980)$ exchange contributions to the nucleon–nucleon interaction.¹ The corresponding interaction terms take the form $\sim g_{\sigma NN} \sigma \bar{N} N$ and $\sim g_{a_0 NN} a_0^a \bar{N} \tau_a N$. These mesons couple to the Lorentz scalar density in the isoscalar and isovector channels, respectively. According to large- N_c counting, the couplings scale as $g_{\sigma NN} \sim N_c$ and $g_{a_0 NN} \sim O(1)$. More quantitatively, meson–exchange potentials ([Stoks et al., 1994](#)) yield $g_{\sigma NN}/g_{a_0 NN} \simeq 3.8$, which is consistent with this large- N_c expectation.

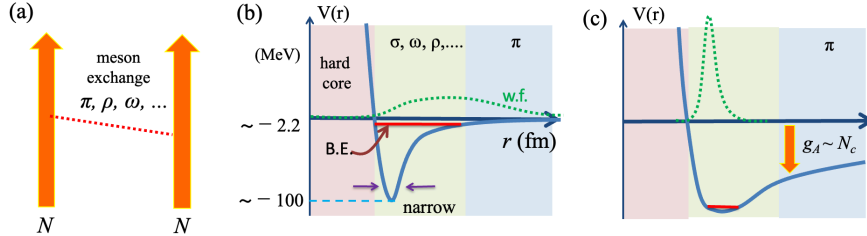


Fig. 3 Schematic nuclear forces and their large N_c implications. (a) Meson-exchange picture of the nucleon-nucleon interaction. (b) Qualitative shape of the nuclear potential at $N_c = 3$, showing a hard core, intermediate-range attraction, and long-range pion exchange, leading to a shallow bound state. (c) Extrapolation to large N_c , where the axial coupling $g_A \sim N_c$ enhances the long-range pion-exchange interaction, leading to a deeply bound two-nucleon state. As a consequence, nuclear matter is expected to form a crystal at large N_c .

4.2 The nucleon axial charge

The above discussions with vector and scalar mesons exchanges are relatively simple as one can estimate the (vector) charges and Lorentz scalar charges rather easily. A more subtle and intriguing channel is the axial (-vector) charges to which pions couple. In non-relativistic operator languages, the nucleon axial charge is proportional to the spin-isospin operator

$$G_{ia} \equiv \sigma_i \tau_a, \quad (6)$$

which, together with the spin and isospin generators, forms an $SU(4)$ spin-flavor algebra (Gervais and Sakita, 1984; Dashen et al., 1994). In the standard quark model, it is known that the ground-state baryons are described by a completely symmetric spin-flavor wave function for which one finds $\langle N | G_{ia} | N \rangle \sim N_c$ (Manohar, 1984). As a consequence, the axial coupling scales as $g_A \sim N_c$, and the pion-nucleon coupling is parametrically enhanced. The Goldberger-Treiman relation $g_{\pi NN} f_\pi = g_A m_N$ (f_π : pion decay constant, m_N : nucleon mass) suggests $g_{\pi NN} \sim N_c^{3/2}$ since $f_\pi \sim N_c^{1/2}$ and $M_N \sim N_c$ (Hidaka et al., 2011).

Regarding $g_{\pi NN}$ as strong coupling leads to a picture of large pion clouds (coherent pions) surrounding the nucleon core. Those pions take a specific field configuration, chiral soliton, with a topological charge one which is identified as a baryon number. The most famous construction is the Skyrme (Skyrme, 1961, 1962) which is the classical solution of the Lagrangian (for a review, Zahed and Brown (1986))

$$\mathcal{L} = \frac{f_\pi^2}{4} \text{tr}(\partial_\mu U \partial^\mu U^\dagger) + \frac{1}{32e^2} \text{tr} \left([U^\dagger \partial_\mu U, U^\dagger \partial_\nu U]^2 \right) + \frac{f_\pi^2 m_\pi^2}{4} \text{tr}(U + U^\dagger - 2), \quad U = e^{i\pi_a \tau_a / f_\pi}. \quad (7)$$

Assuming fields π to be classical or large amplitude fields, the quadratic and quartic derivative terms are balanced to yield soliton solutions. The spin and isospin quantum number of this soliton is the mixture of several baryon species. This is energetically possible since, in conventional quark models at large N_c , the nucleon and Δ mass splitting comes from the color magnetic interactions of $\alpha_s \sim 1/N_c$, meaning that their masses become degenerate at large N_c . Hence, in order to describe a nucleon, one needs to project the nucleon quantum number from the classical soliton (projection after variation) (Adkins et al., 1983). There are several upgraded versions of the Skyrme model which include vector mesons such as ρ and ω mesons. A more elegant construction is the instanton construction in holographic QCD with infinite towers of mesons included (e.g., Sakai and Sugimoto (2005); Hata et al. (2007); Hong et al. (2007)).

4.3 Nuclear binding

While the large N_c baryons and the resulting soliton construction include a lot of interesting physics, the direct application to the nuclear physics is subtle. In nuclear physics, there emerges an unnaturally small scale of a few MeV which is typical in nuclear binding energies (Fig. 3). In nuclear matter near the saturation density, the kinetic energy of nucleon, $\sim \vec{p}^2/m_N \sim \Lambda_{\text{QCD}}/N_c$, is typically several tens of MeV, while the binding energy seems to be $\sim \Lambda_{\text{QCD}}/N_c^2$. For this to happen, the kinetic and potential energies should largely cancel, so the potential energy should be $\sim \Lambda_{\text{QCD}}/N_c$, especially at long distance. If we consider the large pion fields of $\sim N_c$, the attractive potential at long distance is too large. Pushing this description to many-body systems leads to crystals of chiral solitons (Klebanov, 1985), since the potential dominates over the kinetic energy and it is energetically more favorable for nucleons to take the fixed locations. In contrast, the empirical nuclear matter is like a liquid where the kinetic and potential energies are comparable.

To summarize this section, the $1/N_c$ classifications for baryon-baryon interactions work in many channels, but the channel involving the axial charges needs special care. This issue propagates to descriptions of many-body problems. In practice, treating g_A as order unity provides a reasonable picture for dense nuclear matter (Hidaka et al., 2011). In the following, we proceed to denser matter within the picture of $g_A \sim 1$, without rigorous justifications.

¹Here σ denotes an effective scalar-isoscalar degree of freedom commonly employed in meson-exchange descriptions of nuclear forces, rather than a narrow fundamental resonance.

5 Hot matter at large N_c

Now we extend the $1/N_c$ expansion to hot matter. The state of matter can be specified by thermodynamic variables, baryon chemical potential μ_B and temperature T , and the pressure $P(\mu_B, T) = \mu_B n_B + Ts - \varepsilon$ (n_B : baryon density; s : entropy density; ε : energy density). Our understanding of the hot regime of QCD has matured, thanks to the combined use of lattice QCD, heavy-ion experiments, and physics-inspired effective models (for reviews, e.g., [Braun-Munzinger et al. \(2016\)](#); [Shuryak \(2017\)](#)). Equations of state, transport properties, hadronic correlations in hot medium, and so on, have been examined in detail.

First we consider a hot matter at $\mu_B = 0$. At finite temperature, the abundance of thermally excited hadrons is controlled by the Boltzmann factor $e^{-\beta E_n}$ ($\beta = 1/T$: inverse temperature) times the degeneracy factor including spins, isospins, and so on. At large N_c , masses of mesons and glueballs are $\sim N_c^0 \Lambda_{\text{QCD}}$, while baryon masses are $\sim N_c \Lambda_{\text{QCD}}$. Thus, at $T \ll N_c \Lambda_{\text{QCD}}$, a hot matter is dominated by a gas of mesons and glueballs in which interactions are suppressed by $1/N_c$. Since the decay width of mesons and glueballs are suppressed by $1/N_c$, these particles may be regarded as quasi-particles. This allows us to write the pressure simply as

$$P(T) = -T \sum_n \int_{\vec{p}} \ln(1 - e^{-\beta E_n(\vec{p})}), \quad E_n(\vec{p}) = \sqrt{\vec{p}^2 + m_n^2}, \quad (8)$$

where n characterizes a hadronic state with the mass m_n . We sum over all possible hadronic states as independent. There are no quantities which manifestly depend on N_c , and hence the resultant pressure is $\sim N_c^0$.

At large excitation energies, the number of hadronic states grows rapidly because there are many possible stringy excitations, i.e., excitations of color-electric flux connecting colored objects such as quarks and gluons. There are open strings connecting quarks and antiquarks, and also closed strings making glueball states. At large N_c , string breaking and string interactions are suppressed, so that these string excitations can be counted as independent states. The string models for hadrons suggest that the density of hadronic states, or entropy, exhibits an exponential growth,

$$\rho(m) \sim m^{-a} e^{m/T_H}, \quad (9)$$

where T_H is called the Hagedorn temperature ([Hagedorn, 1965](#)). Replacing the discrete sum over hadronic states by an integral over the mass, the pressure takes the schematic form

$$P(T) \sim - \int dm \rho(m) \int_{\vec{p}} \ln(1 - e^{-\beta \sqrt{\vec{p}^2 + m^2}}) \sim \int dm m^{-a} e^{m(\frac{1}{T_H} - \frac{1}{T})} \int_{\vec{p}} e^{-\beta \frac{\vec{p}^2}{2m} + \dots}. \quad (10)$$

As T approaches T_H from below, the exponential growth of $\rho(m)$ overcomes the Boltzmann suppression, and the partition function ceases to be well-defined.

This ill-defined behavior comes from overcounting of states; we have treated all hadrons and the associated strings as independent. When hadrons or the associated color flux strongly overlap, however, we should imagine the condensation of the color fluxes that overcomes the suppression factor $1/N_c$ ([Polyakov, 1978](#); [Gross et al., 1981](#)). Such a matter forms a colored background within which quarks and gluons directly contribute to the thermodynamics, see quark models augmented by Polyakov loops as successful examples ([Fukushima, 2004](#); [Ratti et al., 2006](#); [Schaefer et al., 2007](#); [Fukushima and Skokov, 2017](#)). In this sense, the Hagedorn temperature may be viewed as a limiting temperature of the hadronic description. Once the colored background is formed, the pressure is dominated by gluons of $\sim N_c^2$ which is regarded as bigger than quark contributions of $\sim N_f N_c$. This pressure is substantially larger than the hadronic pressure of $\sim N_c^0$, discriminating the confined and deconfined phases. If quark contributions are neglected, one finds the deconfinement temperature $T_{\text{deco}} \sim 270$ MeV.

While the above large N_c descriptions capture the qualitative trends of confinement-deconfinement transitions, there are substantial corrections at $N_c = 3$. The quantitative aspects have been examined by lattice Monte-Carlo results. Indeed, it is established that the transition from hadronic to QGP phase is smooth crossover ([Aoki et al., 2006](#)) which begins at the pseudo-critical temperature $T_c \simeq 155$ MeV ([Bhattacharya et al., 2014](#)). Around T_c , the entropy density is $s \simeq 2\text{-}3 \text{ fm}^{-3}$, suggesting that two- or three-quark composites, mesons and baryons with the radii $\sim 0.5\text{-}1$ fm, begin to overlap. This is supported by the fact that the hadron resonance gas model, including substantial baryon contributions at $N_c = 3$, works very well to T_c ([Karsch et al., 2003](#); [Huovinen and Petreczky, 2010](#)), but beyond which the pressure (entropy) is overestimated. Various number susceptibilities including those of charm quarks begin to change at the common temperature T_c ([Ding et al., 2016](#)); this trend is consistent with the picture of the string condensation at large N_c which form a background universal for all flavors. What is specific at $N_c = 3$ is that the color-flux is mainly brought by mesons and baryons.

To summarize, while the large- N_c descriptions are not quantitatively precise, they provide very useful qualitative guidelines and organizing principles for hot QCD.

6 Cold, dense matter at large N_c

In the cold, dense regime, a matter is formed when the baryon chemical potential $\mu_B = N_c \mu_q$ (μ_q : quark chemical potential) exceeds the nucleon mass $m_N \sim N_c \Lambda_{\text{QCD}}$ (minus the binding energy), or equivalently when μ_q exceeds the effective quark mass $M_q \sim \Lambda_{\text{QCD}}$. As announced in Sec. 4.3, we assume that nuclear matter remains liquid even at large N_c , provided that $g_A \sim 1$.

We first quickly review findings since 2010 for cold, dense matter in the real-world QCD. The major sources of empirical information are

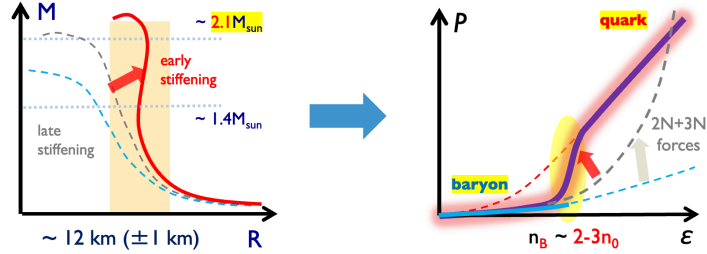


Fig. 4 Observational constraints on neutron star M - R relations and the corresponding inference which suggests that the EOS stiffens rapidly around $2-3n_0$ ($n_0 \simeq 0.16 \text{ fm}^{-3}$: nuclear saturation density \simeq nucleon density in typical nuclei) and approaches the quark matter behavior with $P \simeq \epsilon/3$.

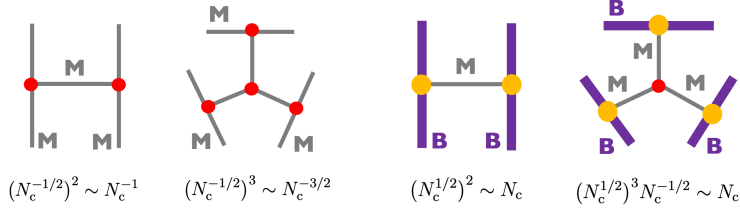


Fig. 5 Large- N_c scaling of many-body forces in mesonic and baryonic systems. For mesons, the N -body vertices scale as $\sim N_c^{-N/2}$ and are increasingly suppressed for larger N , implying that hot mesonic matter is dominated by two-body interactions. For baryons, in contrast, the N -body vertices can remain as large as the two-body vertices, scaling as $\sim N_c$. As a result, many-body forces play a crucial role in dense baryonic matter, in sharp contrast to mesonic matter.

the nuclear physics around saturation density $n_0 \simeq 0.16 \text{ fm}^{-3}$ and neutron star constraints. In particular, the mass-radius M - R measurements for neutron stars, which have drastically improved since the discovery of a two-solar mass neutron star, have provided a lot of information for the QCD equations of state (EOS) for $n_B = 1-5n_0$. We then discuss several concepts deduced from large N_c arguments which are useful to formulate theoretical problems.

6.1 Implications from empirical constraints

EOS of matter and M - R relations of neutron stars have one-to-one correspondence. If the M - R curve is determined precisely, one can directly obtain the EOS and from which we can infer the microphysics of dense matter (Lattimer and Prakash, 2001; Alford et al., 2007; Bauswein et al., 2019; Baym et al., 2018; Annala et al., 2020).

One of the most important concepts in neutron star EOS is the stiffness of matter or the relative magnitude of pressure (P) with respect to the energy density (ϵ). The energy density is the source of gravitational contraction while the pressure counteracts on the compression of matter. A stiff (soft) EOS has a large (small) P at a given ϵ ; when P grows more rapidly (slowly) with increasing n_B and ϵ , it means that the matter is harder (easier) to be compressed. For instance, a matter of non-relativistic baryons leads to $\epsilon \sim m_N n_B + n_B^{5/3}/m_N$, and the resulting pressure is $P = n_B^2 \partial(\epsilon/n_B)/\partial n_B \sim n_B^{5/3}/m_N$, suppressed by its large mass. Hence $P \ll \epsilon$, very soft. For a matter of relativistic particles, $\epsilon \sim n_B^{4/3}$, the pressure is $P \sim n_B^{4/3} \sim \epsilon$ and hence the EOS is stiff. In the relativistic limit, one can find $P = \epsilon/3$ after eliminating n_B in favor of ϵ .

One of symbolic findings in recent neutron star observations is the peak in the (adiabatic) sound speed, $c_s = (\partial P/\partial \epsilon)^{1/2}$, exceeding the value of the relativistic limit, $c_s = (1/3)^{1/2}$ (Masuda et al., 2013; Kojo et al., 2015; Bedaque and Steiner, 2015; Ma and Rho, 2020). The Bayesian inference, constrained by nuclear physics, neutron star observations, and perturbative QCD at very high density, suggests that the peak appears at densities intermediate between baryonic and quark matter, $n_B \sim 2-5n_0$ (e.g., Brandes et al. (2023); Han et al. (2023)). If we consider transitions from baryonic to quark matter as distinct *phase* transitions, it is difficult to explain the sound speed peak or the rapid stiffening. Indeed, at first order phase transitions, the pressure is constant but the energy density jumps discontinuously, leading to $c_s = 0$. For this reason, the possibility of the quark-hadron crossover has been explored as a viable scenario (Masuda et al., 2013; Baym et al., 2018). Explaining rapid stiffening from the baryonic to quark matter regimes is one of key issues in the contemporary dense QCD physics.

6.2 Quarkyonic matter

The application of large N_c leads to a new look into the relation between baryonic and quark matter. Below we introduce the concept of *quarkyonic* matter (McLerran and Pisarski, 2007), a hypothetical phase of QCD at large N_c , characterized by a quark Fermi sea coexisting with confining gluodynamics.

One significant difference from hot matter is that interactions among baryons are very strong. As we discussed in Sec. 4, two-body forces between baryons are $\sim N_c$. This trend continues to three-, four-, and more-body forces. For instance, in the meson exchange picture for

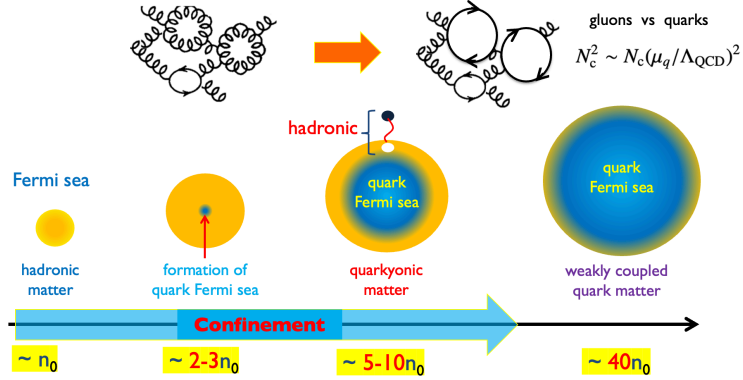


Fig. 6 A possible scenario for the evolution of strongly interacting matter from the nuclear to the quark regime. At large N_c , gluonic contributions dominate over quark screening effects up to $\mu_q \sim N_c^{1/2} \Lambda_{QCD}$, allowing confinement to persist at high density. As a result, a quarkyonic regime emerges, characterized by a quark Fermi sea in the bulk with confined, hadronic excitations near the Fermi surface. Estimates for the real world with $N_c = 3$ are shown as a guideline for relevant densities.

three-baryon forces, there is an extra $N_c^{-1/2}$ suppression factor at a three-meson vertex but there is also an extra $N_c^{1/2}$ enhancement factor in the meson-baryon coupling (Fig. 5). As a result, the three-baryon forces can be at the same order as two-baryon forces. In the dilute regime, what suppresses many-baryon forces is the probability that many-baryons meet at once; for short-range (contact-like) interactions, the n -body forces scale as $V_{n\text{-body}} \sim N_c \Lambda_{QCD} \times (n_B/\Lambda_{QCD}^3)^n$ where Λ_{QCD}^{-1} is the typical length scale for the baryon size or the range of meson-exchanges.

Once μ_B exceeds m_N , the baryon density increases quickly; the baryon Fermi energy $E_F = \sqrt{m_N^2 + p_F^2} \simeq m_N + p_F^2/2m_N$ (p_F : baryon Fermi momentum) changes only slightly for increasing p_F so that little growth of μ_B allows p_F or $n_B \sim p_F^3$ to increase rapidly. Hence, within a small window of μ_B , the baryonic matter changes from the dilute to dense regime, and those baryons interact strongly. Remembering that quarks are exchanged in meson-exchange processes, it is difficult to differentiate strongly interacting baryonic matter from quark matter.

In terms of EOS, these two descriptions of matter have interesting duality. The discussion is simple for the energy density; both baryonic and quark matter scale as $\varepsilon \sim N_c \Lambda_{QCD}^4$ for $n_B \sim \Lambda_{QCD}^3$. In baryonic descriptions, the energy density is dominated by the mass and potential energies, $\varepsilon_B \sim m_N n_B + \sum_n N_c \Lambda_{QCD}^4 \times (n_B/\Lambda_{QCD}^3)^n$, where the kinetic term of $\sim 1/N_c$ is neglected. In quark descriptions, there are N_c quarks so that the energy scales like $\varepsilon_q \sim N_c (E_q + V_q) n_B$ where V_q is the average potential energy for a single quark. We note that the quark density for a given color is equal to baryon density, i.e., $n_q^R = n_q^G = n_q^B = \dots = n_B$, since a single baryon contains one quark for a given color.

Meanwhile the pressure is more non-trivial. The pressure can be computed as $P = n_B^2 \partial(\varepsilon/n_B)/\partial n_B$. For baryonic matter, the mass energy, with the $\varepsilon_{\text{mass}}/n_B \sim m_N$, drops off from the pressure, and the interaction terms dominate the pressure,

$$P_B \sim \sum_n (n-1) N_c \Lambda_{QCD}^4 \times (n_B/\Lambda_{QCD}^3)^n. \quad (11)$$

Meanwhile, in quark descriptions, the pressure is $P_q \sim N_c n_B^{4/3}$ in the relativistic limit and $P_q \sim N_c n_B^{5/3}/M_q$ for the non-relativistic case. At $n_B \sim \Lambda_{QCD}^3$, baryonic and quark descriptions can be matched in both the energy density and pressure. In this regard, the thermodynamic properties at large N_c may smoothly change from the hadronic to quark matter.

The formation of quark matter, however, by itself does not imply deconfinement of colors or vanishing of color-flux tubes. At large N_c , confinement persists up to parametrically large baryon chemical potential, $\mu_q \sim N_c^{1/2} \Lambda_{QCD}$, since quark loop effects are suppressed by $1/N_c$. This estimate is based on the balance between the gluonic quantum fluctuations of $\sim N_c^2$ with the quark quantum fluctuations of $\sim N_c(\mu_q/\Lambda_{QCD})^2$ (Fig. 6). The enhancement factor of $(\mu_q/\Lambda_{QCD})^2$ comes from the enlarged phase space near the Fermi surface, $\sim 4\pi p_F^2 \Lambda_{QCD} \sim 4\pi \mu_q^2 \Lambda_{QCD}$, larger than the phase space in the vacuum cases, $\sim \Lambda_{QCD}^3$. More explicitly, one can compute the Debye screening mass, $m_D \sim g_s \mu_q$, for electric gluons and compare it with Λ_{QCD} . When $\mu_q \sim N_c^{1/2} \Lambda_{QCD}$, the color screening caused by quarks cuts off gluons in the infrared, and then the dynamics becomes weak coupling from high to low momentum transfer processes.

The above arguments suggest that, in the window between $\mu_q \sim \Lambda_{QCD}$ and $\mu_q \sim N_c^{1/2} \Lambda_{QCD}$, we have a matter in which natural degrees of freedom are quarks, but confining gluons persist. Since quarks fill the Fermi sea equally for each color, bulk quark matter can remain globally color-singlet, and the formation of a quark Fermi sea does not contradict confinement. Such quark matter with confining gluons is called *quarkyonic* matter (McLerran and Pisarski, 2007). In this matter, a colored-excitation on top of the color-singlet Fermi sea must be combined with other colored excitations until the resulting composite becomes color-singlet. Hence, it is convenient to describe quarkyonic matter as quark matter in the bulk part but baryonic matter near the Fermi surface.

An important application of the quarkyonic matter scenario is the construction of EOS (McLerran and Reddy, 2019). Assuming quarks confined inside baryons but increasing density, it has been argued that quarks inevitably form the quark Fermi sea at low momenta, leading to quark scaling of the EOS (Kojo, 2021). In terms of baryons, baryons under-occupy states at low momenta and largely pushed to higher momenta to avoid the breaking of the quark Pauli principle. The onset of the quark Fermi sea triggers the rapid stiffening, as requested from neutron star constraints. This was explicitly demonstrated for an ideal, analytically tractable model constructed in Fujimoto et al. (2024).

In reality of $N_c = 3$, whether the window for quarkyonic matter exists or is large enough is not known and further discussions are called for. Especially, color-superconducting phases (for a review, [Alford et al. \(2008\)](#)), which are plausible at high density, are entirely missed in the large N_c limit. Even so, the large N_c arguments have offers new perspectives on dense matter; they certainly sharpened the conception of confinement-deconfinement and also brought our attention to new ideas that would explain rapid stiffening of EOS.

7 Two-color QCD and isospin QCD as laboratories of dense QCD

So far we have seen that the $1/N_c$ expansion provides us with useful classification schemes from hadronic physics to extreme matter. The next step is to examine the concepts developed in the large N_c , e.g., quarkyonic matter, by studying theories where one can work out various computations explicitly. Two color QCD is an example of such theories since the lattice Monte-Carlo simulations can be performed for cold, dense matter, without encountering the notorious sign-problem ([Hands et al., 1999](#); [Iida and Itou, 2022](#)). In this theory, baryonic matters are made of bosonic baryons (color-singlet diquarks) and differ from those in real-world QCD. Nevertheless, at densities high enough for hadrons to strongly overlap, quark matter should be formed and here the difference in colors may not be so important. Another useful theory is isospin QCD, i.e., QCD at finite isospin but zero baryon chemical potentials. In both QC_2D and QCD_I , dense hadronic matter is made of bosons, color-singlet diquarks for QC_2D and mesons with isospin charges (e.g., charged pions) for QCD_I . Below we consider QC_2D unless otherwise stated, but for EOS we quote results in QCD_I where simulations cover densities up to the pQCD domain ([Abbott et al., 2023](#)). At finite temperature and zero baryon chemical potential, the qualitative trend is very similar to the real-world QCD; finite temperature transitions at zero chemical potentials are crossover for quark masses which have been used for lattice simulations. Hence below we mostly focus on the physics at finite density.

7.1 Pseudo-real representations and Pauli–Gürsey symmetry

To identify relevant effective degrees of freedom in QC_2D , it is essential to know the symmetry breaking pattern and the associated Nambu–Goldstone (NG) bosons. For massless quarks, the real-world QCD has the $SU(N_f)_L \times SU(N_f)_R \times U(1)_B$ global symmetry. In QC_2D , the symmetry is enlarged due to the pseudo-real nature of the fundamental representation of $SU(2)_c$, which relates fundamental and anti-fundamental color representations ([Kogut et al., 2000](#)). Historically, the particle–antiparticle mixing underlying this symmetry was first identified by Pauli ([Pauli, 1957](#)), while its interpretation as an internal continuous symmetry was later formalized by Gürsey ([Gürsey, 1958](#)).

Using σ_A ($A = 1, 2, 3$) as the generators of $SU(2)_c$, we define the charge-conjugated quark field as (C denotes the charge-conjugation matrix)

$$(\tilde{q}_{L/R})_i^a \equiv C_{ij} \sigma_2^{ab} (\tilde{q}_{R/L})_j^b. \quad (12)$$

By construction, $\tilde{q}_{L/R}$ transforms as a left-/right-handed quark under Lorentz and flavor transformations, while transforming in the fundamental representation under color rotations. The latter follows from

$$\sigma_2 q^* \rightarrow \sigma_2 U^* q^* = \sigma_2 U^* \sigma_2 \sigma_2 q^* = U(\sigma_2 q^*), \quad \sigma_2 \sigma_a^* \sigma_2 = -\sigma_a, \quad (13)$$

where $U \in SU(2)_c$. Using the identity $C \gamma_\mu C^{-1} = -\gamma_\mu^T$, the Lagrangian for massless quarks ($D_\mu = \partial_\mu + ig_s A_\mu$) can be rewritten as

$$\mathcal{L}_q = \bar{q}_L i \mathbb{D} q_L + \bar{q}_R i \mathbb{D} q_R = \bar{q}_L i \mathbb{D} q_L + \bar{q}_L i \mathbb{D} \tilde{q}_L = \bar{\Psi}_L i \mathbb{D} \Psi_L, \quad \Psi_L \equiv (q_L, \tilde{q}_L)^T = (u_L, d_L, \tilde{u}_L, \tilde{d}_L)^T. \quad (14)$$

The field Ψ_L transforms as a left-handed fermion under Lorentz transformations. Alternatively, one may work with Ψ_R instead of Ψ_L .

Under the usual chiral rotations $SU(N_f)_L \times SU(N_f)_R$, the fields transform independently as $q_L \rightarrow e^{i\theta_L^f T_f} q_L$ and $\tilde{q}_L \rightarrow e^{i\theta_L^f T_f} \tilde{q}_L$, leaving the Lagrangian invariant. In addition, the Lagrangian is invariant under the enlarged $SU(2N_f)$ transformation $\Psi_L \rightarrow e^{i\theta_L^f T_f} \Psi_L$, where T_f are the generators of $SU(2N_f)$. This enlarged $SU(2N_f)$ symmetry, which mixes quarks and charge-conjugated antiquarks, is known as the Pauli–Gürsey symmetry ([Pauli, 1957](#); [Gürsey, 1958](#)), and strongly constrains the dynamics of mesons and diquarks. We note that the $U(1)_B$ symmetry, which acts differently on quarks and anti-quarks, is already embedded in $SU(2N_f)$. Therefore, in the massless case, the number of generators is $(2N_f)^2 - 1$, which equals 15 for $N_f = 2$.

Upon introducing the quark mass term, it is tempting to employ both Ψ_L and Ψ_R . But their chiral transformations are not independent by construction and hence there is no $SU(2N_f)_L \times SU(2N_f)_R$ symmetry even in the massless limit. Using Ψ_L fields alone, the mass term takes the form

$$\bar{q}_L \hat{m}_q q_L + \bar{q}_R \hat{m}_q q_L = \Psi_L^T C \sigma_2 \begin{bmatrix} 0 & -\hat{m}_q \\ \hat{m}_q & 0 \end{bmatrix} \Psi_L, \quad (15)$$

where \hat{m}_q denotes the quark mass matrix.

From here on, we restrict ourselves to the $N_f = 2$ case and assume degenerate current quark masses, $m_u = m_d$. The mass term explicitly breaks the global flavor $SU(4)$ symmetry to $Sp(4) \simeq SO(5)$, which is defined as the subgroup of unitary transformations satisfying

$$U^T \Sigma_0 U = \Sigma_0, \quad \Sigma_0 = \begin{bmatrix} 0 & \mathbf{1}_2 \\ -\mathbf{1}_2 & 0 \end{bmatrix}. \quad (16)$$

Likewise, the formation of the chiral condensate $\langle \bar{u}u \rangle = \langle \bar{d}d \rangle$ spontaneously breaks the symmetry as $SU(4) \rightarrow Sp(4)$. Since the number of

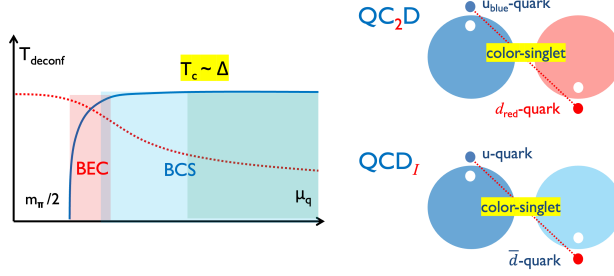


Fig. 7 The phase diagram for QC₂D (QCD_I). Color singlet diquarks (charged pions π_+) begin to condense at $\mu = \mu_q = m_\pi/2$ ($\mu = \mu_I/2$). The dense matter is created first in the BEC regime and crossover to the BCS regime.

broken generators is $15 - 10 = 5$, five NG bosons emerge. These NG bosons form a five-dimensional multiplet of $SO(5)$ with a common mass m_π . They consist of three pions, together with a Lorentz-scalar, flavor-singlet diquark and anti-diquark.

7.2 Phase structure

At finite baryon density, the qualitative features of hadronic matter are substantially modified. In particular, the presence of a nonzero baryon chemical potential μ_B explicitly breaks the $Sp(4)$ symmetry down to $SU(2) \times U(1)_B$, since μ_B differentiates quarks and anti-quarks. Below we assume the current quark mass to be nonzero so that the chiral symmetry is explicitly broken.

Shown in Fig. 7 is the phase diagram for QC₂D (which can be also used for QCD_I after slight modifications). When the baryon chemical potential reaches the diquark mass, $\mu_B = m_\pi$ (or equivalently $\mu_q = m_\pi/2$), diquarks begin to form Bose-Einstein condensates, thereby spontaneously breaking the $U(1)_B$ symmetry. The condensed diquarks are composed of u - and d -quarks in the spatial s -wave, spin-singlet, and flavor-singlet channel.

As the baryon density increases, diquarks eventually overlap and quarks inside those diquarks become important. Those quarks form the Fermi sea and the system is more naturally interpreted as quark matter rather than hadronic matter. Similarly, the diquark condensation changes from the BEC to the Bardeen-Copper-Schrieffer (BCS) regime (see e.g., Sun et al. (2007); von Smekal (2012)). This transition is a BEC-BCS crossover, with no change in symmetry and no discontinuity in thermodynamic quantities.

These low temperature phases with the diquark condensates can be clearly distinguished from the high temperature phases without the diquark condensates, since $U(1)_B$ symmetry is broken in the former but not in the latter. This situation differs from chiral transitions where a small but explicit breaking due to the quark mass exists and the spontaneous symmetry breaking is only an approximate concept.

Although the BEC-BCS crossover does not involve any symmetry change, the relevant degrees of freedom gradually shift from hadronic to quark-like ones. This change becomes particularly important for the equation of state, where Pauli blocking and quark occupation effects play a crucial role.

7.3 Color-singlet quark gap, screening, and gluons

We consider the mean-field spectra of quarks in the BCS regime and examine the impacts on the low energy gluon dynamics. We assume the Yukawa coupling between quarks and (condensed) diquarks (d_q),

$$\frac{g}{2} \langle d_q \rangle \epsilon_{ij} \epsilon_{ab} [(\bar{q} C)_i^a i \gamma_5 q_j^b] + \text{h.c.} = -\frac{g}{2} \langle d_q \rangle [\bar{q}_C \sigma_2 \tau_2 i \gamma_5 q] + \text{h.c.} = \bar{\psi} \begin{bmatrix} 0 & i \gamma_5 \Delta \\ -i \gamma_5 \Delta & 0 \end{bmatrix} \psi, \quad \psi = \frac{1}{\sqrt{2}} \begin{pmatrix} q \\ \sigma_2 \tau_2 q_C \end{pmatrix}, \quad (17)$$

where $q_C = C \bar{q}^T$ and $\Delta = g \langle d_q \rangle$. Here ψ is called the Nambu-Gor'kov spinor. The mean-field effective Lagrangian is

$$\mathcal{L}_{\text{MF}} = \bar{\psi}(p) \begin{bmatrix} p + \mu \gamma_0 - m_q & i \gamma_5 \Delta \\ -i \gamma_5 \Delta & p - \mu \gamma_0 - m_q \end{bmatrix} \psi(p). \quad (18)$$

Diagonalizing the matrix, one finds the spectra $\epsilon_{p/a}(\vec{p}) = \sqrt{(E_{\vec{p}} \mp \mu_q)^2 + \Delta^2}$ with $E_{\vec{p}} = \sqrt{\vec{p}^2 + m_q^2}$. The gap Δ is the minimum energy to place a quark on top of the quark Fermi sea.

This gap for quark excitations has important impacts on the Debye (electric) screening in colors. The Debye screening mass for gluons can be estimated by computing quark loops coupled to gluon propagators (see, e.g., Rischke (2000a,b)). For $\Delta = 0$, the polarization loop at low momentum \vec{k} is dominated by particle-hole excitations,

$$\Pi_{\text{ph}}(\vec{k}) \sim g_s^2 \int_{\vec{p}} \frac{\Theta(E_{\vec{p}+\vec{k}} - \mu_q) \Theta(\mu_q - E_{\vec{p}}) + \Theta(\mu_q - E_{\vec{p}+\vec{k}}) \Theta(E_{\vec{p}} - \mu_q)}{|E_{\vec{p}+\vec{k}} - \mu_q| + |E_{\vec{p}} - \mu_q|} \sim g_s^2 \int_{\vec{p}} \frac{\vec{v} \cdot \vec{k} \delta(E_{\vec{p}} - \mu_q)}{E_{\vec{p}+\vec{k}} - E_{\vec{p}}} \sim g_s^2 p_F E_F + O(\vec{k}^2). \quad (19)$$

Thus, in the static and long-wavelength limit, $\Pi_{\text{ph}}(\vec{k})$ approaches a constant Debye mass, $m_D^2 \sim (g_s \mu_q)^2$. The key observation is that, in the integrand, both the numerator and denominator are vanishing for $\vec{k} \rightarrow 0$, but the ratio remains finite.

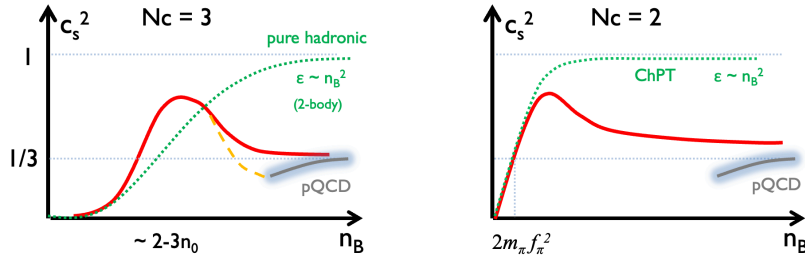


Fig. 8 The density evolution of squared sound speed c_s^2 for three- and two-color QCD. (i) For three colors, a matter made of non-relativistic baryons is soft at low density but rapidly becomes stiff around $n_B \sim 2-3n_0$. How c_s^2 approaches the pQCD estimate at high density is not well-known. (ii) For two colors, EOS of light diquarks become quickly dominated by interactions.

In contrast, in the presence of a quark gap Δ , the particle-hole excitation energy is bounded from below by $\varepsilon_p(\vec{p} + \vec{k}) + \varepsilon_p(\vec{p}) \geq 2\Delta$, i.e., the energy denominator in Eq. (19) becomes finite at $\vec{k} \rightarrow 0$. As a result, the static polarization vanishes in the infrared, and the Debye screening disappears. Hence, the gluon propagators $D_g(k)$ in the infrared, with $|\vec{k}| \leq \Delta$, are protected from the in-medium screening effects. This can leave the non-perturbative gluons even in high density quark matter, a system as discussed in the quarkyonic matter scenario. The lattice simulations indeed seem to be consistent with this observation (Boz et al., 2019).

The presence of the gap by itself does not mean the absence of the color screening. What is special for QC₂D is that the condensate is color-singlet, which guarantees that the numerator, characterized by the quark wavefunctions, vanishes in the limit $\vec{k} \rightarrow 0$ (see, e.g., Kojo and Baym (2014)). If the diquark condensate is colored, as in the color-superconductivity, both the numerator and denominator are nonzero, leaving the Debye mass of $\sim g_s \mu_q$.

As for the magnetic screening, the screening mass vanishes as far as the condensate does not have colors. Hence in QC₂D magnetic gluons in the infrared are also protected (as in the normal phase). This vanishing is achieved by mutual cancellations among the particle-hole and particle-antiparticle contributions which are constrained by the gauge invariance (see, e.g., Kojo and Baym (2014)). In contrast, in the color-superconducting phase in QCD, this cancellation does not hold and the magnetic (Meissner) mass is generated.

Concerning diquark condensed phases, the gluon dynamics in QC₂D cannot be immediately transferred to real-world QCD, since the color structure of the condensates is fundamentally different. Whether gluons in dense QCD remain non-perturbative is therefore a quantitative question, and further studies are needed to estimate the density window where non-perturbative gluon dynamics may persist.

7.4 Equations of state

With the rapid progress in neutron star observations, QC₂D has attracted renewed interest in the context of the stiffening of EOS (Kojo and Suenaga, 2022). As discussed in Sec. 6.1, neutron star data suggest the presence of a peak in the sound speed squared exceeding the conformal limit $c_s^2 = 1/3$. While several phenomenological models had indicated such behavior, it remained unclear whether these results reflected genuine physics or artifacts of specific models and uncontrolled extrapolations beyond the domain of applicability of low density EOS. The first reliable evidence for a sound-speed peak came from lattice simulations of QC₂D performed by Iida and Itou (Iida and Itou, 2022). Similar behavior was also confirmed in QCD₁ (Brandt et al., 2023; Abbott et al., 2023). Qualitative comparisons of c_s^2 for QCD and QC₂D (QCD₁) are shown in Fig. 8.

7.4.1 Dilute regime

In the dilute regime near $\mu_B \sim m_\pi$, the EOS is well-described by the chiral perturbation theory (ChPT), a low-energy effective field theory of QCD based on the spontaneous breaking of chiral symmetry (Weinberg, 1979; Gasser and Leutwyler, 1984, 1985). Computing $P(\mu_B)$ first, subsequently the number and energy densities can be computed as (Kogut et al., 2000)

$$P(\mu_B) = \frac{f_\pi^2}{2} \mu_B^2 \left(1 - \frac{m_\pi^2}{\mu_B^2}\right)^2 \quad \rightarrow \quad n_B = \frac{\partial P}{\partial \mu_B} = f_\pi^2 \mu_B \left(1 - \frac{m_\pi^4}{\mu_B^4}\right), \quad \varepsilon = \mu_B n_B - P = \frac{f_\pi^2}{2} \left(\mu_B^2 + 2m_\pi^2 - \frac{3m_\pi^4}{\mu_B^2}\right). \quad (20)$$

A more intuitive form can be derived by rewriting ε as a function of n_B . Near the onset, we expand $\mu_B \simeq m_\pi + \delta\mu_B$, express $n_B \simeq 4f_\pi^2 \delta\mu_B + O(\delta\mu_B^2)$, and then eliminate $\delta\mu_B$ of P in favor of n_B . In the dilute regime, the resulting expression consists of the mass energy and two-body repulsive terms,

$$\varepsilon \simeq m_\pi n_B + \frac{n_B^2}{8f_\pi^2} + O(n_B^3). \quad (21)$$

Unlike the real-world QCD, (i) the baryon is so light that the non-relativistic regime ends within a small density interval; (ii) there is no kinetic term like $\sim n_B^{5/3}/m_\pi$ since, in bosonic systems, there is no Fermi momentum for baryons.

The mass and interaction terms become comparable when $n_B \sim 2m_\pi f_\pi^2$ beyond which the validity of the above simple expression would be lost. If we assume $m_\pi = 140$ MeV and $f_\pi = 90$ MeV, the density for the breakdown is $2m_\pi f_\pi^2 \simeq 0.30 \text{ fm}^{-3}$, which is about a half of the density where diquarks (pions) with the radii ~ 0.7 fm to spatially overlap. The pressure as a function of n_B and the sound speed is computed

as

$$P \simeq \frac{n_B^2}{8f_\pi^2}, \quad c_s^2 = \frac{dP/dn_B}{d\varepsilon/dn_B} \simeq \frac{n_B}{4m_\pi f_\pi^2 + n_B}. \quad (22)$$

The c_s^2 increases with n_B from zero, exceeds the conformal limit $1/3$ at $n_B \simeq 2m_\pi f_\pi^2$, and asymptotically reaches the causal upperbound $c_s^2 = 1$ (the sound speed should not exceed the speed of light; see, e.g., (Zeldovich, 1962)). But $c_s^2 > 1/3$ is achieved only beyond the supposed breakdown scale $n_B \sim 2m_\pi f_\pi^2$ and hence the validity of Eq. (22) is questionable. In particular, the limit $c_s^2 \rightarrow 1$ at large n_B is a mere artifact of extrapolating the dilute chiral expansion beyond its domain of validity. It is worth mentioning that, if the EOS were dominated by an N -body interaction term of the form $\varepsilon \sim n_B^N$, one would formally obtain the asymptotic behavior $c_s^2 \sim N - 1$, which exceeds the causal bound $c_s^2 = 1$ for $N > 2$ (see, e.g., Kojo (2025)). This observation illustrates that a naive power-series expansion in n_B , when extrapolated to high density, is incompatible with basic relativistic constraints. Therefore, the structure of the EOS must be qualitatively modified in the dense regime, where new degrees of freedom and nonperturbative dynamics become essential.

7.4.2 Dense regime

In the dense regime after baryons overlap, one expects the importance of quark degrees of freedom. In the relativistic limit, the kinetic energy is so large that it dominates over the interaction energy. The EOS behaves as $P(\mu_q) \sim \mu_q^4$ or, equivalently, $\varepsilon(n_B) \sim n_B^{4/3}$.

At high density $\mu_q > 1\text{-}2$ GeV, one expects the applicability of perturbative QCD (pQCD) (Freedman and McLerran, 1977; Kurkela et al., 2010; Gorda et al., 2023). The pressure of perturbative QCD at asymptotically high density can be written as

$$P(\mu_q) = \frac{N_c N_f}{12\pi^2} \mu_q^4 \left[1 - a_2 \alpha_s(\mu_q) - a_4 \alpha_s^2(\mu_q) - a'_4 \alpha_s^2(\mu_q) \ln \alpha_s(\mu_q) + \dots \right], \quad (23)$$

where $a_i > 0$ are numerical coefficients depending on N_f and the renormalization scale for α_s is taken to be $\sim \mu_q$. The logarithm $\ln \alpha_s$ comes from the ratio between μ_q and the Debye mass $m_D \sim g_s \mu_q$. In pQCD, the intrinsic scale of QCD, Λ_{QCD} , appears only through α_s . From this expression one can compute c_s^2 which, as μ_q increases, approaches the conformal limit $1/3$ from below. Correspondingly, pQCD suggests $c_s^2 < 1/3$ in the density range where perturbation theory is expected to become applicable, $\mu_q \sim 1\text{-}2$ GeV.

How $c_s^2 < 1/3$ at high density can be consistent with $c_s^2 > 1/3$ at low density is an important question in contemporary dense QCD studies. One possible scenario is to add (non-perturbative) power corrections, of the form $\sim \mu_q^2 \Lambda_{\text{QCD}}^2$, to the pQCD EOS. Since Λ_{QCD} is non-analytic as a function of α_s , the expansion of α_s cannot capture such corrections. A simple EOS with the power corrections and the resultant c_s^2 are (e.g., Chiba and Kojo (2024))

$$P(\mu_q) = c_0 \mu_q^4 + c_2 \mu_q^2 \Lambda_{\text{QCD}}^2 \quad \rightarrow \quad c_s^2 = \frac{2c_0 \mu_q^2 + c_2 \Lambda_{\text{QCD}}^2}{6c_0 \mu_q^2 + c_2 \Lambda_{\text{QCD}}^2}. \quad (24)$$

Assuming $c_2 > 0$, we find $c_s^2 > 1/3$ which approaches the conformal limit from above. Increasing density in the BEC regime and reducing density in the BCS regime both lead to the sound speed peak in the crossover domain.

How the power corrections arise and what physics is responsible for Λ_{QCD} depend on theories. One plausible origin for Λ_{QCD} is the gap Δ in diquark condensed phases. In the BCS theory the presence of the gap adds a term like $\delta P \sim +\mu_q^2 \Delta^2$ to the pressure or more intuitively leads to the energy reduction, $\delta E \sim -p_F^2 \Delta^2$, with p_F^2 comes from the area of the Fermi surface, $\sim 4\pi p_F^2$.

If Δ depends on μ_q only weakly and is comparable to Λ_{QCD} , the BCS-type EOS immediately supplies the power corrections $\mu_q^2 \Lambda_{\text{QCD}}^2$, smoothly matching the low density EOS having the c_s^2 peak with the high density counterpart. This picture is supported for the case of isospin QCD (QCD_I), where lattice simulations up to the pQCD domain are available (Abbott et al., 2023). The data shows that c_s^2 has a peak at low density and remains larger than $1/3$ at $\mu_q \sim 1$ GeV. The data is well-reproduced for a nearly constant Δ of $\sim 200\text{-}300$ MeV.

To derive the gap Δ at high density, it is natural to apply weak coupling approaches (Son, 1999). Several analyses showed that the overall size and density dependence of Δ are sensitive to theories we consider; Δ for the pion condensed phase in QCD_I, diquark condensed phase in QC₂D, and color-superconducting phase in the real-world QCD, can be considerably different, since different numerical factors appear in the exponent (Wang and Rischke, 2002; Fujimoto, 2024). For QCD_I, the weak coupling estimate is consistent with the lattice data, while in QC₂D the estimate seems smaller by a factor of $\sim 2\text{-}4$. The prediction for two-flavor pairing in QCD is Δ of a several MeV, too small for power corrections to alter the trend of pQCD. In the real-world QCD, how to reconcile the c_s^2 peak inferred from neutron star data and the weak coupling results at very high density remains an important question (Fukushima and Minato, 2025).

8 Summary

In this review we have surveyed various aspects of QCD and QCD-like theories from the viewpoint of the $1/N_c$ expansion, covering its applications to hadron physics, nuclear interactions, hot QCD, and dense matter. Despite $N_c = 3$, the $1/N_c$ expansion provides a powerful organizing principle that reveals common structures across seemingly different regimes.

Dense QCD stands out as a particularly challenging arena for the $1/N_c$ approach, due to the sign problem, the limited experimental access, and the restricted applicability of effective theories. At the same time, it is precisely in this regime that the interplay between perturbative and nonperturbative physics becomes most transparent.

In this context, QCD with two colors plays a special role. Because baryons are bosonic and lattice simulations at finite density are feasible, QC₂D provides a theoretically controlled laboratory to study dense QCD matter from the dilute regime to asymptotically high

density. The EOS of QC₂D allows for a direct comparison between ChPT, lattice results, and perturbative expectations.

A particularly illuminating observable is the sound speed. Lattice simulations of QC₂D show that the sound speed exceeds the conformal limit at intermediate densities, a feature that cannot be explained by perturbative QCD alone. Interestingly, neutron star observations suggest a similar behavior in real QCD, indicating that the emergence of a sound-speed peak may be a generic feature of dense QCD matter, largely independent of the number of colors.

These findings highlight the importance of intermediate-density physics, where a rearrangement of degrees of freedom and nonperturbative effects become essential. Comparing theories with different numbers of colors thus provides valuable insight into the structure of dense QCD and helps to bridge the gap between controlled theoretical limits and real-world strongly correlated matter.

Acknowledgments

This work was supported by JSPS KAK-ENHI Grant No. 23K03377.

See Also: article title article title

References

Abbott R, Detmold W, Romero-López F, Davoudi Z, Illa M, Parreño A, Perry RJ, Shanahan PE and Wagman ML (NPLQCD) (2023). Lattice quantum chromodynamics at large isospin density. *Phys. Rev. D* 108 (11): 114506. doi:10.1103/PhysRevD.108.114506. 2307.15014.

Adkins GS, Nappi CR and Witten E (1983). Static Properties of Nucleons in the Skyrme Model. *Nucl. Phys. B* 228: 552. doi:10.1016/0550-3213(83)90559-X.

Alford M, Blaschke D, Drago A, Klahn T, Pagliara G and Schaffner-Bielich J (2007). Quark matter in compact stars? *Nature* 445: E7–E8. doi:10.1038/nature05582. astro-ph/0606524.

Alford MG, Schmitt A, Rajagopal K and Schäfer T (2008). Color superconductivity in dense quark matter. *Rev. Mod. Phys.* 80: 1455–1515. doi:10.1103/RevModPhys.80.1455. 0709.4635.

Annala E, Gorda T, Kurkela A, Näättilä J and Vuorinen A (2020). Evidence for quark-matter cores in massive neutron stars. *Nature Phys.* 16 (9): 907–910. doi:10.1038/s41567-020-0914-9. 1903.09121.

Aoki Y, Endrodi G, Fodor Z, Katz SD and Szabo KK (2006). The Order of the quantum chromodynamics transition predicted by the standard model of particle physics. *Nature* 443: 675–678. doi:10.1038/nature05120. hep-lat/0611014.

Bauswein A, Bastian NUF, Blaschke DB, Chatzioannou K, Clark JA, Fischer T and Oertel M (2019). Identifying a first-order phase transition in neutron star mergers through gravitational waves. *Phys. Rev. Lett.* 122 (6): 061102. doi:10.1103/PhysRevLett.122.061102. 1809.01116.

Baym G, Hatsuda T, Kojo T, Powell PD, Song Y and Takatsuka T (2018). From hadrons to quarks in neutron stars: a review. *Rept. Prog. Phys.* 81 (5): 056902. doi:10.1088/1361-6633/aaae14. 1707.04966.

Bedaque P and Steiner AW (2015). Sound velocity bound and neutron stars. *Phys. Rev. Lett.* 114 (3): 031103. doi:10.1103/PhysRevLett.114.031103. 1408.5116.

Bhattacharya T, Buchoff MI, Christ NH, Ding HT, Gupta R, Jung C, Karsch F, Lin Z, Mawhinney R, McGlynn G, Mukherjee S, Murphy D, Petreczky P, Schroeder C, Soltz R, Vranas P and Yin H (2014). The qcd phase transition with physical-mass, chiral quarks. *Phys. Rev. D* 90: 094503. doi:10.1103/PhysRevD.90.094503. 1402.5175.

Boz T, Hajizadeh O, Maas A and Skullerud JI (2019). Finite-density gauge correlation functions in QC2D. *Phys. Rev. D* 99 (7): 074514. doi:10.1103/PhysRevD.99.074514. 1812.08517.

Brandes L, Weise W and Kaiser N (2023). Inference of the sound speed and related properties of neutron stars. *Phys. Rev. D* 107 (1): 014011. doi:10.1103/PhysRevD.107.014011. 2208.03026.

Brandt BB, Cuteri F and Endrodi G (2023). Equation of state and speed of sound of isospin-asymmetric QCD on the lattice. *JHEP* 07: 055. doi:10.1007/JHEP07(2023)055. 2212.14016.

Braun-Munzinger P, Koch V, Schäfer T and Stachel J (2016). Properties of hot and dense matter from relativistic heavy ion collisions. *Phys. Rep.* 621: 76–126.

Callan Jr. CG, Coote N and Gross DJ (1976). Two-Dimensional Yang-Mills Theory: A Model of Quark Confinement. *Phys. Rev. D* 13: 1649. doi:10.1103/PhysRevD.13.1649.

Chiba R and Kojo T (2024). Sound velocity peak and conformality in isospin QCD. *Phys. Rev. D* 109 (7): 076006. doi:10.1103/PhysRevD.109.076006. 2304.13920.

Coleman S (1985). *Aspects of Symmetry*, Cambridge University Press.

Dashen RF, Jenkins EE and Manohar AV (1994). The 1/N(c) expansion for baryons. *Phys. Rev. D* 49: 4713. doi:10.1103/PhysRevD.51.2489. [Erratum: Phys. Rev. D 51, 2489 (1995)], hep-ph/9310379.

Ding HT, Banerjee D and et al. (2016). Charm quark contribution to the qcd equation of state. *Phys. Rev. D* 94: 114503. doi:10.1103/PhysRevD.94.114503. 1608.03230.

Freedman BA and McLerran LD (1977). Fermions and Gauge Vector Mesons at Finite Temperature and Density. 3. The Ground State Energy of a Relativistic Quark Gas. *Phys. Rev. D* 16: 1169. doi:10.1103/PhysRevD.16.1169.

Fujimoto Y (2024). Enhanced contribution of the pairing gap to the QCD equation of state at large isospin chemical potential. *Phys. Rev. D* 109 (5): 054035. doi:10.1103/PhysRevD.109.054035. 2312.11443.

Fujimoto Y, Kojo T and McLerran LD (2024). Momentum Shell in Quarkyonic Matter from Explicit Duality: A Dual Model for Cold, Dense QCD. *Phys. Rev. Lett.* 132 (11): 112701. doi:10.1103/PhysRevLett.132.112701. 2306.04304.

Fukushima K (2004). Chiral effective model with the Polyakov loop. *Phys. Lett. B* 591: 277–284. doi:10.1016/j.physletb.2004.04.027. hep-ph/0310121.

Fukushima K and Hatsuda T (2011). The phase diagram of dense QCD. *Rept. Prog. Phys.* 74: 014001. doi:10.1088/0034-4885/74/1/014001. 1005.4814.

Fukushima K and Minato S (2025). Speed of sound and trace anomaly in a unified treatment of the two-color diquark superfluid, the pion-condensed high-isospin matter, and the 2SC quark matter. *Phys. Rev. D* 111 (9): 094006. doi:10.1103/PhysRevD.111.094006. 2411.03781.

Fukushima K and Skokov V (2017). Polyakov loop modeling for hot QCD. *Prog. Part. Nucl. Phys.* 96: 154–199. doi:10.1016/j.ppnp.2017.05.002. 1705.00718.

Gasser J and Leutwyler H (1984). Chiral perturbation theory to one loop. *Annals Phys.* 158: 142–210. doi:10.1016/0003-4916(84)90242-2.

Gasser J and Leutwyler H (1985). Chiral perturbation theory: Expansions in the mass of the strange quark. *Nucl. Phys. B* 250: 465–516. doi:10.1016/0550-3213(85)90492-4.

Gervais JL and Sakita B (1984). Large N QCD Baryon Dynamics: Exact Results from Its Relation to the Static Strong Coupling Theory. *Phys. Rev. Lett.* 52: 87. doi:10.1103/PhysRevLett.52.87.

Gorda T, Paatelainen R, Säppi S and Seppänen K (2023). Equation of State of Cold Quark Matter to $O(\alpha_s^3 \ln \alpha_s)$. *Phys. Rev. Lett.* 131 (18): 181902. doi:10.1103/PhysRevLett.131.181902. 2307.08734.

Gross DJ, Pisarski RD and Yaffe LG (1981). QCD and Instantons at Finite Temperature. *Rev. Mod. Phys.* 53: 43. doi:10.1103/RevModPhys.53.43.

Gürsey F (1958). Relation of charge independence and baryon conservation to Pauli's transformation. *Nuovo Cim.* 7 (3): 411–415. doi:10.1007/bf02747705.

Hagedorn R (1965). Statistical thermodynamics of strong interactions at high-energies. *Nuovo Cim. Suppl.* 3: 147–186.

Han MZ, Huang YJ, Tang SP and Fan YZ (2023). Plausible presence of new state in neutron stars with masses above 0.98MTOV. *Sci. Bull.* 68: 913–919. doi:10.1016/j.scib.2023.04.007. 2207.13613.

Hands S, Kogut JB, Lombardo MP and Morrison SE (1999). Symmetries and spectrum of SU(2) lattice gauge theory at finite chemical potential. *Nucl. Phys. B* 558: 327–346. doi:10.1016/S0550-3213(99)00364-8. hep-lat/9902034.

Hata H, Sakai T, Sugimoto S and Yamato S (2007). Baryons from instantons in holographic QCD. *Prog. Theor. Phys.* 117: 1157. doi:10.1143/PTP.117.1157. hep-th/0701280.

Hidaka Y, Kojo T, McLerran L and Pisarski RD (2011). The Dichotomous Nucleon: Some Radical Conjectures for the Large N_c Limit. *Nucl. Phys. A* 852: 155–174. doi:10.1016/j.nuclphysa.2011.01.008. 1004.2261.

Hong DK, Rho M, Yee HU and Yi P (2007). Chiral Dynamics of Baryons from String Theory. *Phys. Rev. D* 76: 061901. doi:10.1103/PhysRevD.76.061901. hep-th/0701276.

Huovinen P and Petreczky P (2010). Qcd equation of state and hadron resonance gas. *Nucl. Phys. A* 837: 26–53. doi:10.1016/j.nuclphysa.2010.02.015. 0912.2541.

Iida K and Itou E (2022). Velocity of sound beyond the high-density relativistic limit from lattice simulation of dense two-color QCD. *PTEP* 2022 (11): 111B01. doi:10.1093/ptep/ptac137. 2207.01253.

Kaplan DB and Savage MJ (1996). The Spin flavor dependence of nuclear forces from large n QCD. *Phys. Lett. B* 365: 244–251. doi:10.1016/0370-2693(95)01277-X. hep-ph/9509371.

Karsch F, Tawfik A and Redlich K (2003). Thermodynamics at non-zero baryon number density: A comparison of lattice and hadron resonance gas model calculations. *Phys. Lett. B* 571: 67–74. doi:10.1016/S0370-2693(03)00947-3. hep-ph/0104088.

Klebanov IR (1985). Nuclear Matter in the Skyrme Model. *Nucl. Phys. B* 262: 133–143. doi:10.1016/0550-3213(85)90068-9.

Kogut JB, Stephanov MA, Toublan D, Verbaarschot JJM and Zhitnitsky A (2000). QCD - like theories at finite baryon density. *Nucl. Phys. B* 582: 477–513. doi:10.1016/S0550-3213(00)00242-X. hep-ph/0001171.

Kojo T (2021). Stiffening of matter in quark-hadron continuity. *Phys. Rev. D* 104 (7): 074005. doi:10.1103/PhysRevD.104.074005. 2106.06687.

Kojo T (2025). Stiffening of matter in quark–hadron continuity: A mini-review. *J. Subatomic Part. Cosmol.* 4: 100088. doi:10.1016/j.jspc.2025.100088. 2412.20442.

Kojo T and Baym G (2014). Color screening in cold quark matter. *Phys. Rev. D* 89 (12): 125008. doi:10.1103/PhysRevD.89.125008. 1404.1346.

Kojo T and Suenaga D (2022). Peaks of sound velocity in two color dense QCD: Quark saturation effects and semishort range correlations. *Phys. Rev. D* 105 (7): 076001. doi:10.1103/PhysRevD.105.076001. 2110.02100.

Kojo T, Powell PD, Song Y and Baym G (2015). Phenomenological QCD equation of state for massive neutron stars. *Phys. Rev. D* 91 (4): 045003. doi:10.1103/PhysRevD.91.045003. 1412.1108.

Kurkela A, Romatschke P and Vuorinen A (2010). Cold Quark Matter. *Phys. Rev. D* 81: 105021. doi:10.1103/PhysRevD.81.105021. 0912.1856.

Lattimer JM and Prakash M (2001). Neutron star structure and the equation of state. *Astrophys. J.* 550: 426. doi:10.1086/319702. astro-ph/0002232.

Ma YL and Rho M (2020). Towards the hadron–quark continuity via a topology change in compact stars. *Prog. Part. Nucl. Phys.* 113: 103791. doi:10.1016/j.ppnp.2020.103791. 1909.05889.

Manohar AV (1984). Equivalence of the Chiral Soliton and Quark Models in Large N . *Nucl. Phys. B* 248: 19. doi:10.1016/0550-3213(84)90584-4.

Masuda K, Hatsuda T and Takatsuka T (2013). Hadron–quark crossover and massive hybrid stars. *PTEP* 2013 (7): 073D01. doi:10.1093/ptep/ptt045. 1212.6803.

McLerran L and Pisarski RD (2007). Phases of cold, dense quarks at large $N(c)$. *Nucl. Phys. A* 796: 83–100. doi:10.1016/j.nuclphysa.2007.08.013. 0706.2191.

McLerran L and Reddy S (2019). Quarkyonic Matter and Neutron Stars. *Phys. Rev. Lett.* 122 (12): 122701. doi:10.1103/PhysRevLett.122.122701. 1811.12503.

Pauli W (1957). On the conservation of the lepton charge. *Il Nuovo Cimento* 6 (1): 204–215. doi:10.1007/BF02827771.

Pelaez JR (2004). On the Nature of light scalar mesons from their large $N(c)$ behavior. *Phys. Rev. Lett.* 92: 102001. doi:10.1103/PhysRevLett.92.102001. hep-ph/0309292.

Polyakov AM (1978). Thermal Properties of Gauge Fields and Quark Liberation. *Phys. Lett. B* 72: 477–480. doi:10.1016/0370-2693(78)90737-2.

Ratti C, Thaler MA and Weise W (2006). Phases of QCD: Lattice thermodynamics and a field theoretical model. *Phys. Rev. D* 73: 014019. doi:10.1103/PhysRevD.73.014019. hep-ph/0506234.

Rischke DH (2000a). Debye screening and Meissner effect in a three flavor color superconductor. *Phys. Rev. D* 62: 054017. doi:10.1103/PhysRevD.62.054017. nucl-th/0003063.

Rischke DH (2000b). Debye screening and Meissner effect in a two flavor color superconductor. *Phys. Rev. D* 62: 034007. doi:10.1103/PhysRevD.62.034007. nucl-th/0001040.

Sakai T and Sugimoto S (2005). Low energy hadron physics in holographic QCD. *Prog. Theor. Phys.* 113: 843–882. doi:10.1143/PTP.113.843. hep-th/0412141.

Schaefter BJ, Pawłowski JM and Wambach J (2007). The Phase Structure of the Polyakov–Quark-Meson Model. *Phys. Rev. D* 76: 074023. doi:10.1103/PhysRevD.76.074023. 0704.3234.

Shuryak E (2017). Strongly coupled quark-gluon plasma in heavy ion collisions. *Rev. Mod. Phys.* 89: 035001. doi:10.1103/RevModPhys.89.035001. 1412.8393.

Skyrme THR (1961). A Nonlinear field theory. *Proc. Roy. Soc. Lond. A* 260: 127–138. doi:10.1088/rspa.1961.0018.

Skyrme THR (1962). A Unified Field Theory of Mesons and Baryons. *Nucl. Phys.* 31: 556–569. doi:10.1016/0029-5582(62)90775-7.

Son DT (1999). Superconductivity by long range color magnetic interaction in high density quark matter. *Phys. Rev. D* 59: 094019. doi:10.1103/

PhysRevD.59.094019. hep-ph/9812287.

Stoks VGJ, Klomp RAM, Terheggen CPF and de Swart JJ (1994). Construction of high quality N N potential models. *Phys. Rev. C* 49: 2950–2962. doi:10.1103/PhysRevC.49.2950. nucl-th/9406039.

Sun Gf, He L and Zhuang P (2007). BEC-BCS crossover in the Nambu-Jona-Lasinio model of QCD. *Phys. Rev. D* 75: 096004. doi:10.1103/PhysRevD.75.096004. hep-ph/0703159.

't Hooft G (1974). A Planar Diagram Theory for Strong Interactions. *Nucl. Phys. B* 72: 461. doi:10.1016/0550-3213(74)90154-0.

von Smekal L (2012). Universal Aspects of QCD-like Theories. *Nucl. Phys. B Proc. Suppl.* 228: 179–220. doi:10.1016/j.nuclphysbps.2012.06.006. 1205.4205.

Wang Q and Rischke DH (2002). How the quark selfenergy affects the color superconducting gap. *Phys. Rev. D* 65: 054005. doi:10.1103/PhysRevD.65.054005. nucl-th/0110016.

Weinberg S (1979). Phenomenological lagrangians. *Physica A* 96: 327–340. doi:10.1016/0378-4371(79)90223-1.

Weinberg S (2013). Tetraquark Mesons in Large N Quantum Chromodynamics. *Phys. Rev. Lett.* 110: 261601. doi:10.1103/PhysRevLett.110. 261601. 1303.0342.

Wilson KG and Fisher ME (1972). Critical exponents in 3.99 dimensions. *Phys. Rev. Lett.* 28: 240–243. doi:10.1103/PhysRevLett.28.240.

Witten E (1980). THE 1 / N EXPANSION IN ATOMIC AND PARTICLE PHYSICS. *NATO Sci. Ser. B* 59: 403–419. doi:10.1007/978-1-4684-7571-5-21.

Zahed I and Brown GE (1986). The Skyrme Model. *Phys. Rept.* 142: 1–102. doi:10.1016/0370-1573(86)90142-0.

Zeldovich YB (1962). The equation of state at ultrahigh densities and its relativistic limitations. *Soviet Physics JETP* 14: 1143–1147.